



Metallic n-Type Mg_3Sb_2 Single Crystals Demonstrate the Absence of Ionized Impurity Scattering and Enhanced Thermoelectric Performance

Kazuki Imasato,* Chenguang Fu,* Yu Pan, Max Wood, Jimmy Jiahong Kuo, Claudia Felser, and G. Jeffrey Snyder*

$\text{Mg}_3(\text{Sb,Bi})_2$ alloys have recently been discovered as a competitive alternative to the state-of-the-art n-type $\text{Bi}_2(\text{Te,Se})_3$ thermoelectric alloys. Previous theoretical studies predict that single crystals $\text{Mg}_3(\text{Sb,Bi})_2$ can exhibit higher thermoelectric performance near room temperature by eliminating grain boundary resistance. However, the intrinsic Mg defect chemistry makes it challenging to grow n-type $\text{Mg}_3(\text{Sb,Bi})_2$ single crystals. Here, the first thermoelectric properties of n-type Te-doped Mg_3Sb_2 single crystals, synthesized by a combination of Sb-flux method and Mg-vapor annealing, is reported. The electrical conductivity and carrier mobility of single crystals exhibit a metallic behavior with a typical $T^{-1.5}$ dependence, indicating that phonon scattering dominates the charge carrier transport. The absence of any evidence of ionized impurity scattering in Te-doped Mg_3Sb_2 single crystals proves that the thermally activated mobility previously observed in polycrystalline materials is caused by grain boundary resistance. Eliminating this grain boundary resistance in the single crystals results in a large enhancement of the weighted mobility and figure of merit zT by more than 100% near room temperature. This work experimentally demonstrates the accurate understanding of charge-carrier scattering is crucial for developing high-performance thermoelectric materials and indicates that single-crystalline $\text{Mg}_3(\text{Sb,Bi})_2$ solid solutions can exhibit higher zT compared to polycrystalline samples.

n-Type $\text{Mg}_3\text{Sb}_2\text{-Mg}_3\text{Bi}_2$ alloys are one of the most potent thermoelectric materials for low- (near room temperature) to mid-temperature range^[1–9] because of their highly degenerate

conduction band structure^[1,4] and extremely low phonon thermal conductivity.^[10–11] Since the discovery of n-type $\text{Mg}_3\text{Sb}_{1.5}\text{Bi}_{0.5}$ with zT of 1.6 at 700 K in 2016,^[1] extensive research have been conducted to improve their thermoelectric performance via the engineering of the electronic band structure,^[5,12] chemical doping,^[13–16] bonding^[17–19] and modulation of microstructure.^[20–22] The studies of carrier and phonon transport mechanisms have also been carried out in parallel to understand the underlying reasons behind the high thermoelectric performance. However, there is a much-debated topic in n-type polycrystalline $\text{Mg}_3\text{Sb}_2\text{-Mg}_3\text{Bi}_2$ alloys concerning the charge carrier scattering mechanism near room temperature, namely, the origin of the low-temperature electrical conductivity and carrier mobility that increases with temperature. While initially attributed to ionized impurity scattering,^[3,23–25] there has been growing evidence supporting that this low-temperature behavior stems from thermally activated grain-boundary resistance.^[20–22,26]

The effect is more pronounced for Sb-rich alloys, particularly Mg_3Sb_2 .^[5] Additionally, a previous grain boundary resistance model study predicted more than 50% improvement of the room-temperature weighted mobility if the grain boundary resistance is completely removed.^[20] Therefore, studying the thermoelectric properties of metallic n-type single crystals is of paramount importance. On one hand, the elimination of grain boundary effect in metallic single crystals would directly answer whether the ionized impurity scattering detracts from charge carrier transport or not. On the other hand, a full characterization of the thermoelectric transport properties of the single crystals can directly validate the prediction of the grain-boundary resistance model.

Compared to polycrystalline samples, there have been much fewer studies on single crystals of Mg_3Sb_2 and Mg_3Bi_2 .^[27,28] Kim et al. have grown $\text{Mg}_{3-x}\text{Mn}_x\text{Sb}_2$ and $\text{Mg}_3\text{Sb}_{2-x}\text{Bi}_x$ single crystals by Bridgman method.^[29] All the $\text{Mg}_3\text{Sb}_{2-x}\text{Bi}_x$ single crystals with $0 \leq x \leq 2$ exhibited p-type transport behavior. Although $\text{Mg}_{3-x}\text{Mn}_x\text{Sb}_2$ with $x = 0.3$ and 0.4 show a negative Seebeck coefficient, the crystals exhibit only weak n-type behavior with a maximum electron concentration of $1.33 \times 10^{18} \text{ cm}^{-3}$, owing

K. Imasato, M. Wood, J. J. Kuo, Prof. G. J. Snyder
Materials Science & Engineering (MSE)
Northwestern University
Evanston, IL 60208, USA
E-mail: kazuki49a7@gmail.com; jeff.snyder@northwestern.edu

Dr. C. Fu, Dr. Y. Pan, Prof. C. Felser
Department of Solid State Chemistry
Max Planck Institute for Chemical Physics of Solids
01187 Dresden, Germany
E-mail: chenguang.fu@cpfs.mpg.de

The ORCID identification number(s) for the author(s) of this article can be found under <https://doi.org/10.1002/adma.201908218>.

© 2020 The Authors. Published by WILEY-VCH Verlag GmbH & Co. KGaA, Weinheim. This is an open access article under the terms of the Creative Commons Attribution License, which permits use, distribution and reproduction in any medium, provided the original work is properly cited.

DOI: 10.1002/adma.201908218

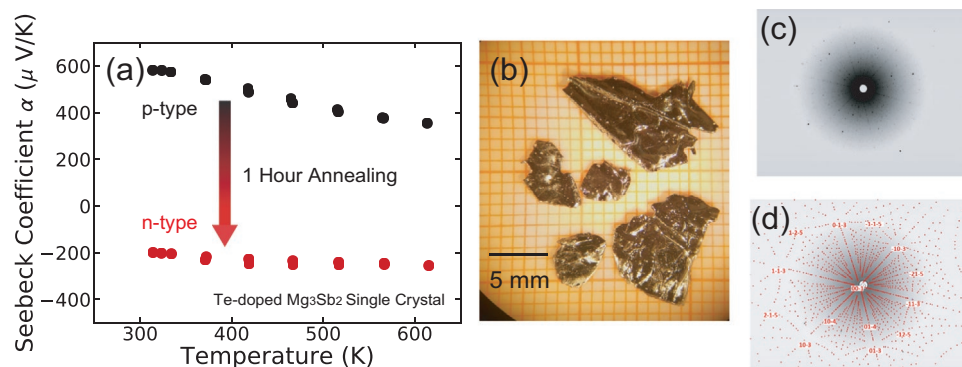


Figure 1. a) Te-doped Mg_3Sb_2 single crystals exhibit a positive Seebeck coefficient (p-type) before annealing and a negative Seebeck coefficient (n-type) after only 1 h of Mg vapor annealing. b) Photograph of crystals as grown out of the Sb-flux (before annealing). The crystals have platelet morphology with faster growth along the ab-plane, consistent with results on p-type crystals.^[28] The typical thickness is 0.2–1.2 mm, and the typical length up to 5–10 mm. c) The X-ray diffraction pattern of the crystals after 16 h of Mg-vapor saturation annealing. Laue diffraction spots are detected indicating the successful synthesis of the n-type single crystals. d) The diffraction pattern can be indexed based on the $P\bar{3}m1$ space group, for incident X-rays perpendicular to the growth plane. The superposed simulated pattern with indices is also given.

to the fact that Mn is not an effective dopant in Mg_3Sb_2 . Xin et al. have grown Mg_3Sb_2 and Mg_3Bi_2 by a self-flux method with Sb and Bi as the flux, respectively, but the crystals also exhibit p-type charge transport behavior.^[28] The reason that heavily doped n-type Mg_3Sb_2 single crystals are difficult to synthesize lies in the peculiar Mg defect chemistry in this system. As the phase boundary mapping study proved,^[2] metallic n-type transport can only be produced in Mg_3Sb_2 when the sample is in equilibrium with elemental Mg. When the chemical potential of Mg in Mg_3Sb_2 is set by elemental Mg, the formation energy of electron-compensating Mg vacancies is increased to the point that extrinsic (impurity) dopants can degenerately dope the material n-type. In polycrystalline samples, this equilibrium with Mg is achieved by putting a small amount of excess Mg into the starting mixture during synthesis. This is nearly impossible for achieving n-type single crystals of Mg_3Sb_2 , as it is generally grown by using an Sb-flux method giving a Mg-poor sample. Growing crystals in Sb flux puts the crystals in equilibrium with Sb and leads to the formation of electron-killing Mg vacancies.

In this study, we have successfully synthesized metallic n-type Te-doped Mg_3Sb_2 single crystals using an Sb-flux growth method followed by Mg saturation annealing.^[21,30] These metallic n-type single crystals enable us to investigate the intrinsic carrier transport mechanism. The electrical conductivity and carrier mobility exhibit a typical $T^{-1.5}$ dependence, demonstrating that phonons dominate the scattering of charge carriers and no evidence of ionized impurity scattering is found. More importantly, these metallic single crystals with grain-boundary resistance removed exhibit a large enhancement of weighted mobility and zT near room temperature by more than 100%, compared to the polycrystalline samples.

Te-doped Mg_3Sb_2 single crystals were first grown out of Sb flux and exhibit weak p-type charge transport properties. Then the as-grown single crystals were sealed into the MgO crucible with elemental Mg. The crucible was heated up to 600 °C in a graphite susceptor in order to produce a high partial pressure of Mg vapor without melting the equilibrating Mg. Once the crystals were equilibrated with Mg, degenerate

(metallic) n-type charge transport behavior is achieved. Detailed experimental procedures can be found elsewhere.^[21,30] As shown in **Figure 1a**, the Seebeck coefficient of the crystals show a transition from p-type charge transport behavior to n-type charge transport behavior after only 1 h Mg saturation annealing. After annealing, the absolute Seebeck coefficient increases with rising temperature, typical of degenerate semiconductors and is consistent with the results obtained previously in polycrystalline samples with similar electron concentrations.^[21] This result combined with previous studies on the polycrystalline samples^[21] indicate that the saturation annealing technique is applicable for obtaining n-type $\text{Mg}_3(\text{Sb,Bi})_2$ crystals, regardless of the crystallinity of the samples (single crystalline or polycrystalline) and their synthetic process (flux method or hot press etc.), if the extrinsic n-type dopants were added in advance. To ensure equilibrium, the Te-doped Mg_3Sb_2 single crystals were annealed for 16 h for the measurements reported here.

The single crystals grown out of Sb-flux are shown in **Figure 1b** with shiny surfaces observed. After saturation annealing, the annealed crystals were checked with back-scattering Laue diffraction (**Figure 1c**). The clear Laue diffraction spots can be indexed based on the $P\bar{3}m1$ space group as demonstrated by the superposition of the theoretically simulated pattern (**Figure 1d**). This indicates that the single crystallinity does not change after 16 h of Mg-vapor saturation annealing although the carrier type has been reversed from p-type to n-type. The corresponding diffraction spots correspond to the (001) plane implying the plate-like crystals preferentially grow in the plane perpendicular to [001], which is consistent with the previous studies.^[28]

The n-type single crystals provide a good opportunity to study the electrical transport properties and charge carrier scattering mechanism of Mg_3Sb_2 with negligible effect of grain boundaries. The electrical conductivity, shown in **Figure 2a**, is qualitatively different for single crystals compared to polycrystalline samples (grain size of 0.5–10 μm) at low temperature which can be attributed to the effect of grain boundaries. The electrical conductivity of the single crystal (red symbols) shows a $T^{-1.5}$ temperature dependence (decreasing with increasing T

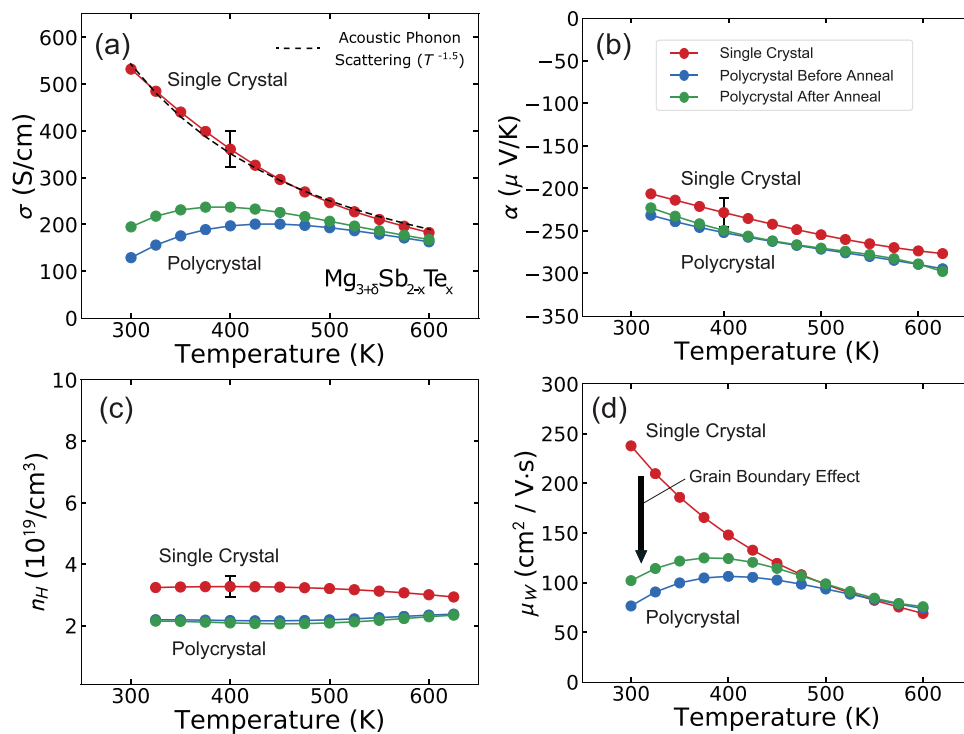


Figure 2. Temperature-dependent transport properties of the single crystal after annealing (red), as compared to the polycrystalline samples (blue: polycrystal as pressed; green: polycrystal after annealing). a) Electrical conductivity (the dashed line shows the temperature dependence expected for acoustic phonon scattering), b) Seebeck coefficient, and c) Hall carrier concentration. d) Single crystals have similar weighted mobility with that of the polycrystalline samples at higher temperatures but have much larger mobility at low temperatures where the grain boundary effect is more pronounced. The weighted mobility at room temperature is more than two times higher in single crystals due to the complete removal of grain boundary resistance.

as expected from simple acoustic phonon scattering theory), demonstrating that the charge carriers are predominantly scattered by phonons. In contrast, the electrical conductivity of the annealed polycrystalline sample (green symbols) increases with temperature around room temperature. This increasing trend of electrical conductivity with temperature in degenerately doped polycrystalline samples was initially attributed to ionized impurity scattering.^[3,23–25] Later observations that the increasing trend of electrical conductivity with temperature is stronger in smaller grain materials^[21–22] lead to a theoretical analysis that this is due to thermally activated charge transport across grain boundaries (grain boundary resistance).^[20] Presumably because all previous (polycrystalline) samples still show some increasing trend of electrical conductivity with temperature below room temperature, many recent reports still claim the predominance of ionized impurity scattering at low temperature.^[3,6,23–25,31–35]

To further check for ionized impurity scattering, we selected another two n-type Mg_3Sb_2 single crystals with lower carrier concentrations (only 1/5 and 1/3 of that of the above-studied single crystal) and measured their electrical resistivity below room temperature, down to 2 K. As shown in **Figure 3**, the electrical resistivity of these two selected single crystal samples continues to decrease with decreasing temperature down to 2 K with a small residual resistivity. This is typical transport behavior of a metal or a degenerate semiconductor.^[36] The absence of an observable decrease in the resistivity

(increase in electrical conductivity or mobility, see Figure S1, Supporting Information) with increasing temperature in single crystals is direct evidence that ionized impurity scattering is not

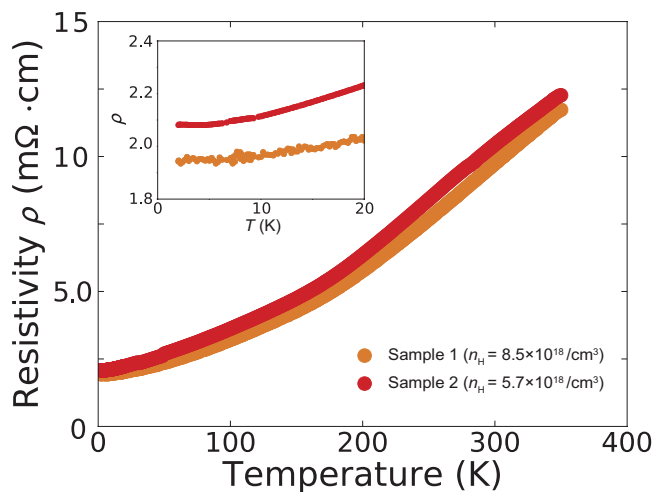


Figure 3. The low-temperature electrical resistivity of Te-doped Mg_3Sb_2 single crystals. The resistivity continuously decreases with decreasing temperature down to 2 K (inset). Since the thermally activated electrical conductivity observed in polycrystalline materials is not observed in single crystals, it can be concluded that the grain boundary resistance, not ionized impurity scattering from the dopant or other homogeneous defects, suppresses the room-temperature electrical conductivity.

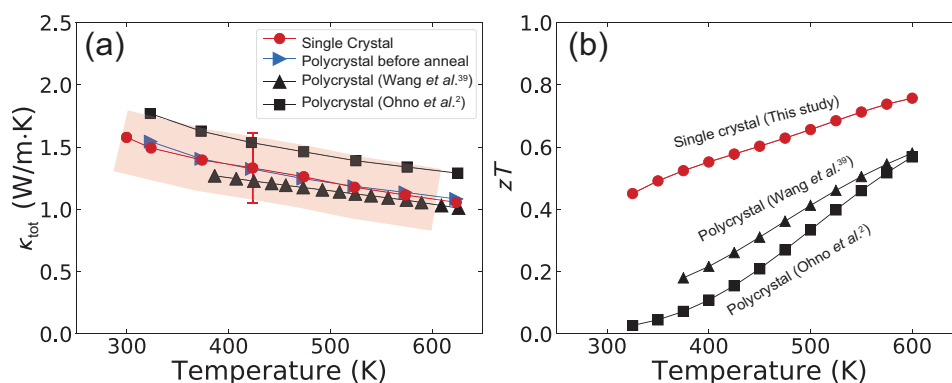


Figure 4. a) Thermal conductivity and b) the zT of Te-doped Mg_3Sb_2 single crystal as a function of temperature. The zT for single crystals are substantially larger than that of polycrystalline samples^[2,39] because of the removal of grain boundary resistance, especially at room temperature. The large measurement uncertainty in the thermal conductivity of single crystal, as indicated in the light red region, is likely due to the small size and irregular shape of the crystal. The higher thermal conductivity in Ohno et al.^[2] is explained by the difference in the Mg content.^[11]

dominant in Mg_3Sb_2 , with charge carrier concentrations near those needed for thermoelectric applications. Thus, through a direct comparison of the electrical conductivities of Te-doped Mg_3Sb_2 single crystals and polycrystalline samples with similar electron concentrations, we can conclude that the increasing trend of electrical conductivity with temperature found only in polycrystalline samples arises from an additional grain-boundary electrical resistance and not because of ionized impurity scattering.

Compared to the annealed polycrystalline samples, the complete removal of the grain boundary effect leads to an approximate 2.5 times higher room-temperature electrical conductivity in the single crystals. The slight deviation of the Seebeck coefficient (Figure 2b) between the single crystal and polycrystalline samples is explained by the small difference in the carrier concentration (Figure 2c), which might come from the difference of actual content of Te dopant. To evaluate the electrical performance independent from carrier concentration, we further analyzed the weighted mobility^[37–38] of the single crystals and polycrystalline samples obtained from the electrical conductivity and Seebeck coefficient measurements.

The weighted mobility of single crystal is approximately two times higher than that of the polycrystalline sample near room temperature due to the elimination of grain boundary resistance (Figure 2d). Since the weighted mobility is independent of the position of the Fermi level or the carrier concentration, it is used to compare the potential electrical performance of thermoelectric materials. Higher weighted mobility corresponds to a higher power factor as well as higher zT , when the carrier concentration is optimized.^[37–38] In contrast to the small difference in Seebeck coefficient, the improvement of electrical conductivity near room temperature is much more pronounced. This improvement in the electrical conductivity due to the elimination of grain boundary resistance results in a significant enhancement of the weighted mobility. On the other hand, at higher temperatures where the grain boundary effect becomes negligible, the weighted mobility of the single crystals exhibits values close to that of the polycrystalline samples.

The large increase of the room-temperature weighted mobility and its $T^{-1.5}$ dependence in the single crystals match the prediction of the grain boundary resistance model.^[20]

The elimination of grain boundaries that predominantly contribute to electrical resistance but does not affect the Seebeck coefficient should be expected to improve the zT , unless there is a proportional increase in thermal conductivity. As single crystals are expected to have higher thermal conductivity than polycrystalline sample, it is imperative to measure thermal conductivity to assess the zT . The thermal conductivity of the single crystals measured along the c -axis, as shown in Figure 4a, is compared to the data of polycrystalline samples. The large measurement uncertainty ($\approx 20\%$ estimated from thickness uncertainty combined with instrument accuracy and sample variation) in the thermal conductivity of the single crystals is likely due to the small size and irregular shape of the crystals (Figure 1b), making an accurate determination of the thermal diffusivity difficult. Within this uncertainty, the thermal conductivity of the single crystals is comparable to that of polycrystalline samples. This result is consistent with previous studies on Mg_3Sb_2 single crystals that indicate its thermal conductivity along the ab -plane which is only about 15% higher than that of polycrystalline samples^[28] and the small effect of grain size on the thermal conductivity due to the inherently short mean free path of phonons.^[22] Using this value, the zT of the single crystals is calculated and shown in Figure 4b. Near room temperature, the zT is significantly higher in the single crystal compared to that of polycrystalline Mg_3Sb_2 .^[2,39] Since the difference in the thermal conductivity is relatively small, the improvement of zT is mainly attributed to the removal of grain-boundary electrical resistance. With increasing temperature, the effect of the grain boundaries gradually diminishes, and the zT values of the single crystal and polycrystalline samples start to converge. It is worth noting that the elimination of the grain boundary effect near room temperature is extremely important since this system is now competitive with commercial Bi_2Te_3 -based thermoelectric materials for low-grade heat recovery and cooling applications.^[5–8,21] Although computational studies predict nearly isotropic thermoelectric transport properties,^[1,18] this should be validated. Here, we only measure c -axis thermal conductivity in single crystals, but as this measured thermal conductivity is similar to polycrystalline samples, we have no reason to believe the thermal conductivity in the ab -plane is significantly different (within the $\approx 30\%$ experimental uncertainty reported here).

Larger, high-quality single crystals will be needed to experimentally determine the anisotropy of Mg_3Sb_2 .

In conclusion, n-type Te-doped Mg_3Sb_2 single crystals were successfully synthesized by a combination of the Sb-flux method and Mg-vapor saturation annealing. The single crystallinity is sustained after 16 h of saturation annealing. Owing to the elimination of grain boundary effect, the n-type single crystals display no thermally-activated grain-boundary electrical-resistance near and below room temperature. This leads to a large enhancement of the weighted mobility and the zT by more than two times near room temperature. Besides the greatly improved thermoelectric performance, the metallic behavior of single crystals is maintained down to 2 K, as evidenced by an additional low-temperature electrical resistivity measurement. These results provide direct evidence that grain boundary scattering, not ionized impurity scattering, is responsible for increasing electrical conductivity with temperature, as is often observed in polycrystalline samples. Moreover, the understanding of Mg_3Sb_2 grain boundary resistance is of paramount importance for future implementation of grain boundary engineering and microstructure optimization toward further development of its thermoelectric performance.

Experimental Section

The single crystals of Te-doped Mg_3Sb_2 were grown by using a self-flux method with Sb flux. Mg (granules, 99.8%), Sb (shots, 99.999%), and Te (pieces, 99.999%) were weighed and mixed with a molar ratio of Mg:Sb:Te of 3.3:7:0.02 and sealed in a tantalum tube in an argon glove box. The tantalum tubes were then sealed in quartz tubes and were held at 850 °C for 30 h. For the crystal growth, the tubes were first quickly cooled down to 750 °C and then slowly cooled down to 630 °C with a rate of 1 °C h⁻¹. The tubes were again heated up to 700 °C for centrifuging to separate the crystals and the Sb flux. The single crystals typically had a platelet shape as shown in Figure 1b with thickness of 0.2–1.2 mm, and the flat face was identified as the ab-plane with typical length of up to 5–10 mm.

Mg Vapor Saturation Annealing Process: The synthesized single crystals were placed into a magnesium oxide crucible. The diameter and height of MgO crucible were both 25 mm. Magnesium turnings (99.98%, Alfa Aesar) were loaded into the crucible together such that the crystals were in contact with elemental Mg. Then, the crucible was placed into a graphite die and covered with graphite foils and a graphite spacer to close the system, so that Mg vapor pressure could be sustained in the crucible. The graphite die was heated up to 600 °C by using induction heating under the flow of argon gas. This was the same procedure used in the polycrystalline study.^[21]

Characterization and Measurement: The synthesized n-type single crystals were analyzed at room temperature by a white backscattering Laue X-ray diffractometer. Laue diffraction spots were detected and could be indexed with a single pattern, which was well superposed with the simulated one (Figure 1d). Electrical and thermal transport measurements were conducted from 300 to 600 K. The electrical resistivity and Hall coefficient were determined using the four-point probe van der Pauw technique with a 2 T magnetic field under high vacuum.^[40] The Seebeck coefficients of the samples were obtained using chromel-Nb thermocouples by applying a temperature gradient across the sample to oscillate between ± 7 K.^[41] The thermal conductivity κ was calculated by $\kappa = D \times C_p \times d$, where d is density and C_p is heat capacity. Thermal diffusivity D was measured by using the laser flash method with a Netzsch LFA 457 under argon flow. The heat capacity values were obtained from a thermodynamic model that fitted to experimental

measurements.^[42] For the low-temperature measurement, PPMS-9T (Quantum Design) was used to measure the longitudinal and Hall resistivities using a standard four-probe method by the ACT option.

Supporting Information

Supporting Information is available from the Wiley Online Library or from the author.

Acknowledgements

This work was supported by the NASA Science Mission Directorate's Radioisotope Power Systems Thermoelectric Technology Development. This work in Dresden was supported by the ERC Advanced Grant No. 742068 "TOPMAT" and the Deutsche Forschungsgemeinschaft (DFG, German Research Foundation)—Projektnummer (392228380). K.I. was partially supported by a Cluster Fellowship from the Institute for Sustainability and Energy at Northwestern (ISEN). C. Fu acknowledges the financial support from the Alexander von Humboldt Foundation.

Conflict of Interest

The authors declare no conflict of interest.

Keywords

acoustic phonon scattering, grain boundaries, Mg_3Bi_2 , Mg_3Sb_2 , weighted mobility

Received: December 15, 2019

Revised: January 20, 2020

Published online: March 1, 2020

- [1] H. Tamaki, H. K. Sato, T. Kanno, *Adv. Mater.* **2016**, *28*, 10182.
- [2] S. Ohno, K. Imasato, S. Anand, H. Tamaki, S. D. Kang, P. Gorai, H. K. Sato, E. S. Toberer, T. Kanno, G. J. Snyder, *Joule* **2018**, *2*, 141.
- [3] J. Shuai, J. Mao, S. Song, Q. Zhu, J. Sun, Y. Wang, R. He, J. Zhou, G. Chen, D. J. Singh, Z. Ren, *Energy Environ. Sci.* **2017**, *10*, 799.
- [4] J. Zhang, L. Song, S. H. Pedersen, H. Yin, L. T. Hung, B. B. Iversen, *Nat. Commun.* **2017**, *8*, 13901.
- [5] K. Imasato, S. D. Kang, G. J. Snyder, *Energy Environ. Sci.* **2019**, *12*, 965.
- [6] X. Shi, C. Sun, Z. Bu, X. Zhang, Y. Wu, S. Lin, W. Li, A. Faghaninia, A. Jain, Y. Pei, *Adv. Sci.* **2019**, *6*, 1802286.
- [7] R. Shu, Y. Zhou, Q. Wang, Z. Han, Y. Zhu, Y. Liu, Y. Chen, M. Gu, W. Xu, Y. Wang, W. Zhang, L. Huang, W. Liu, *Adv. Funct. Mater.* **2019**, *29*, 1807235.
- [8] J. Mao, H. Zhu, Z. Ding, Z. Liu, G. A. Gamage, G. Chen, Z. Ren, *Science* **2019**, *365*, 495.
- [9] F. Zhang, C. Chen, H. Yao, F. Bai, L. Yin, X. Li, S. Li, W. Xue, Y. Wang, F. Cao, X. Liu, J. Sui, Q. Zhang, *Adv. Funct. Mater.* **2019**, 1906143.
- [10] W. Peng, G. Petretto, G.-M. Rignanese, G. Hautier, A. Zevkink, *Joule* **2018**, *2*, 1879.
- [11] K. Imasato, S. Ohno, S. D. Kang, G. J. Snyder, *APL Mater.* **2018**, *6*, 016106.
- [12] K. Imasato, S. D. Kang, S. Ohno, G. J. Snyder, *Mater. Horiz.* **2018**, *5*, 59.

- [13] P. Gorai, B. R. Ortiz, E. S. Toberer, V. Stevanović, *J. Mater. Chem. A* **2018**, *6*, 13806.
- [14] P. Gorai, E. S. Toberer, V. Stevanović, *J. Appl. Phys.* **2019**, *125*, 025105.
- [15] K. Imasato, M. Wood, J. J. Kuo, G. J. Snyder, *J. Mater. Chem. A* **2018**, *6*, 19941.
- [16] J. Zhang, L. Song, K. A. Borup, M. R. V. Jørgensen, B. B. Iversen, *Adv. Energy Mater.* **2018**, *8*, 1702776.
- [17] J. Zhang, L. Song, B. B. Iversen, *npj Comput. Mater.* **2019**, *5*, 42.
- [18] J. Zhang, L. Song, M. Sist, K. Tolborg, B. B. Iversen, *Nat. Commun.* **2018**, *9*, 4716.
- [19] M. Wood, K. Imasato, S. Anand, J. Yang, G. J. Snyder, *J. Mater. Chem. A* **2020**, *8*, 2033.
- [20] J. J. Kuo, S. D. Kang, K. Imasato, H. Tamaki, S. Ohno, T. Kanno, G. J. Snyder, *Energy Environ. Sci.* **2018**, *11*, 429.
- [21] M. Wood, J. J. Kuo, K. Imasato, G. J. Snyder, *Adv. Mater.* **2019**, *31*, 1902337.
- [22] T. Kanno, H. Tamaki, H. K. Sato, S. D. Kang, S. Ohno, K. Imasato, J. J. Kuo, G. J. Snyder, Y. Miyazaki, *Appl. Phys. Lett.* **2018**, *112*, 033903.
- [23] J. Mao, J. Shuai, S. Song, Y. Wu, R. Dally, J. Zhou, Z. Liu, J. Sun, Q. Zhang, C. Dela Cruz, S. Wilson, Y. Pei, D. J. Singh, G. Chen, C. W. Chu, Z. Ren, *Proc. Natl. Acad. Sci. U. S. A.* **2017**, *114*, 10548.
- [24] J. Mao, Y. Wu, S. Song, J. Shuai, Z. Liu, Y. Pei, Z. Ren, *Mater. Today Phys.* **2017**, *3*, 1.
- [25] J. Mao, Y. Wu, S. Song, Q. Zhu, J. Shuai, Z. Liu, Y. Pei, Z. Ren, *ACS Energy Lett.* **2017**, *2*, 2245.
- [26] J. J. Kuo, Y. Yu, S. D. Kang, O. Cojocaru-Miréidin, M. Wuttig, G. J. Snyder, *Adv. Mater. Interfaces* **2019**, *6*, 1900429.
- [27] S. H. Kim, C. M. Kim, Y.-K. Hong, K. I. Sim, J. H. Kim, T. Onimaru, T. Takabatake, M.-H. Jung, *Mater. Res. Express* **2015**, *2*, 055903.
- [28] J. Xin, G. Li, G. Auffermann, H. Borrmann, W. Schnelle, J. Gooth, X. Zhao, T. Zhu, C. Felser, C. Fu, *Mater. Today Phys.* **2018**, *7*, 61.
- [29] S. Kim, C. Kim, Y.-K. Hong, T. Onimaru, K. Suekuni, T. Takabatake, M.-H. Jung, *J. Mater. Chem. A* **2014**, *2*, 12311.
- [30] J. Male, M. T. Agne, A. Goyal, S. Anand, I. T. Witting, V. Stevanović, G. J. Snyder, *Mater. Horiz.* **2019**, *6*, 1444.
- [31] X. Chen, H. Wu, J. Cui, Y. Xiao, Y. Zhang, J. He, Y. Chen, J. Cao, W. Cai, S. J. Pennycook, Z. Liu, L.-D. Zhao, J. Sui, *Nano Energy* **2018**, *52*, 246.
- [32] Z. Ren, J. Shuai, J. Mao, Q. Zhu, S. Song, Y. Ni, S. Chen, *Acta Mater.* **2018**, *143*, 265.
- [33] J. Li, S. Zhang, B. Wang, S. Liu, L. Yue, G. Lu, S. Zheng, *J. Mater. Chem. A* **2018**, *6*, 20454.
- [34] C. Chen, X. Li, S. Li, X. Wang, Z. Zhang, J. Sui, F. Cao, X. Liu, Q. Zhang, *J. Mater. Sci.* **2018**, *53*, 16001.
- [35] X. Shi, T. Zhao, X. Zhang, C. Sun, Z. Chen, S. Lin, W. Li, H. Gu, Y. Pei, *Adv. Mater.* **2019**, *31*, 1903387.
- [36] R. A. Matula, *J. Phys. Chem. Ref. Data* **1979**, *8*, 1147.
- [37] S. Dongmin Kang, G. Jeffrey Snyder, *Nat. Mater.* **2017**, *16*, 252.
- [38] A. Zevalkink, D. M. Smiadak, J. L. Blackburn, A. J. Ferguson, M. L. Chabinyk, O. Delaire, J. Wang, K. Kovnir, J. Martin, L. T. Schelhas, T. D. Sparks, S. D. Kang, M. T. Dylla, G. J. Snyder, B. R. Ortiz, E. S. Toberer, *Appl. Phys. Rev.* **2018**, *5*, 021303.
- [39] Y. Wang, X. Zhang, Y. Wang, H. Liu, J. Zhang, *Phys. Status Solidi A* **2019**, *216*, 1800811.
- [40] K. A. Borup, J. de Boor, H. Wang, F. Drymiotis, F. Gascoin, X. Shi, L. Chen, M. I. Fedorov, E. Müller, B. B. Iversen, G. J. Snyder, *Energy Environ. Sci.* **2015**, *8*, 423.
- [41] S. Iwanaga, E. S. Toberer, A. LaLonde, G. J. Snyder, *Rev. Sci. Instrum.* **2011**, *82*, 063905.
- [42] M. T. Agne, K. Imasato, S. Anand, K. Lee, S. K. Bux, A. Zevalkink, A. J. E. Rettie, D. Y. Chung, M. G. Kanatzidis, G. J. Snyder, *Mater. Today Phys.* **2018**, *6*, 83.